Gašper Fašun
Jožef Predan
Nenad Gubeljak ✉

https://doi.org/10.21278/TOF.483061923
ISSN 1333-1124
eISSN 1849-1391

A FRACTURE-MECHANICS-BASED APPROACH TO THE ANALYSIS OF THE STRUCTURAL INTEGRITY OF A HOWITZER CANNON BARREL

Summary

This study explores the determination of the critical crack depth in howitzer cannon barrels, which is essential for ensuring operational safety, particularly under high-pressure conditions during firing. The fracture-mechanics-based approach, emphasizing the stress intensity factor K_I, is employed to evaluate crack propagation. Specifically, the R6 procedure is applied to assess the failure assessment diagram (FAD), crucial for identifying critical pressures concerning varying crack shapes and depths. The study examines the utilization of high-strength steel 35NiCrMoV12-5 in two distinct heat treatments (materials A and B). Experimental tensile tests and measurements of the critical stress intensity factor K_{IC} were conducted on both materials. The Finite Element Method (FEM) using Abaqus/CAE software was used in combination with experimental results. The FEM model was used to analyses semi-elliptical cracks of different depths and two different shapes. Stress intensity factor distributions along the crack tip were derived, indicating the material resistance to crack propagation.

Key words: *fracture mechanics, howitzer, failure assessment diagram, structure integrity assessment, finite element method*

1. Introduction

For components that are exposed to high loads during their lifetime, such as components in the military or nuclear industry, safety is one of the main aspects to be considered during the design process. The barrel of a howitzer cannon is one such component where this is particularly important, as cannon operators are often near the barrel, which is under extremely high-pressure during firing. In cannon barrels that are under high radial loads during operation, even a small crack can initiate fatigue crack propagation and be fatal to the operators. For this reason, it is important to choose a suitable material with optimal fracture mechanical properties during the design phase.

The fracture-mechanics-based approach is an established practice when dealing with cracks. The main parameter is the stress intensity factor K_I, which has already been used in many studies that analyse pipes or barrels under pressure [1, 2, 3]. It was calculated using various analytical and numerical methods. In the modern era, numerical approaches are used

more and more, among which the finite element method (FEM) is the most popular one in the design of machine components. Leslie et al. used a 2D model for the analysis of the fatigue life of a cannon barrel, determining the critical stress intensity factor K_{IC} in a single point of a crack tip [4]. A similar analysis can be found in the paper by R. A. Mahdavinejad, who also utilized a 2D model to determine K_{IC} at the crack tip of one or multiple cracks in the cannon barrel [5]. A comparable analytical approach for calculating the critical crack length as in [4, 5] was employed in [6, 7], focusing on determining the lifetime of the howitzer cannon. Various crack lengths were analysed in [8], where the authors also determined K_I at a single point using a 2D model.

One of the approaches that can combine K_I with the analysis of different crack depths is to determine a failure assessment diagram (FAD). When determining the FAD, we can choose from many approaches, such as SINTAP [9], ETM [10], BS7910 [11] and R6 [12], being the most common approaches which we will use too. Since it was first published in 1976, the R6 procedure has been expanded by the incorporation of new appendices that focus on specific cases that can be found in everyday industry [13]. An example of using a FAD for the analysis of the integrity of a battle tank's gun barrel is presented in [14], where the authors employed a 2D FEM model and a single shape of a crack to determine the safe operating conditions.

This paper focuses on analysing the integrity of a howitzer cannon barrel while considering two different heat treatments of high strength steel 35NiCrMoV12-5. A symmetrical 3D model of the barrel is presented with different crack shapes and sizes and multiple working conditions, i.e. maximal pressures. By determining FAD diagrams the critical pressures were determined for certain crack dimensions.

2. Material properties

2.1 Chemical properties and heat treatment

In this study, we used an alloy that is known under the designation 35NiCrMoV12-5, whose chemical composition can be seen in Table 1. In general, this alloy is classified as high-strength steel and is intended for structural elements that are subjected to high loads during their lifetime. It is made by the process of electro-slag remelting (ESR) and achieves a high degree of purity. Its density is 7.85 g/cm^3.

Table 1 Chemical composition of 35NiCrMoV12-5 steel in weight % [15]

C	Si	Mn	Cr	Ni	Mo	V	Others
0.39	0.29	0.25	1	3.25	0.6	0.15	Max. Cu=0.15

The same alloy was treated with two different heat treatments that consisted of four stages. The materials are designated as material A and material B. Firstly, material A and material B were subjected to normalization at the temperatures of 870 ºC and 880 ºC, respectively. Following this, both materials underwent identical quenching processes at 860 ºC. The last two stages involved tempering. In the initial tempering stage, materials A and B were tempered at 500 ºC and 600 ºC. The second stage of tempering was carried out at 595 ºC on both materials. The result of different heat treatments can be seen in the tensile test results. The results of the critical fracture toughness K_{IC} of these two materials are comparable.

We have examined the microstructure of both materials and found that the refined microstructure exhibits uniformly distributed tempered martensite in all of the examined areas. The grain size was determined following the ASTM E112 standard, and it was found to be similar in the two heat treatments. The grain size was determined as “grade 6”, which corresponds to a size range of d=45-70 µm. The inclusion sizes were also determined. The largest inclusion that was found for material A had a dimension of d_A=21,9 µm, and for material

B it was d_B=16,9 μm. The results of the EDX analysis showed that the predominant inclusions in the materials are MnS and CaS. In the case of material B the primary inclusions consist of CaS and $CaSO_4$.

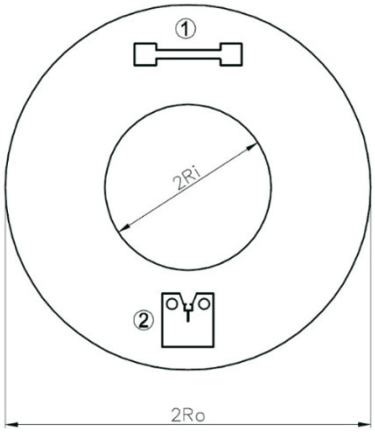

Fig. 1 Distribution of samples for experimental material testing

2.2 Tensile test

The tensile test specimens were produced in accordance with the ISO 6892-1 standard [16]. The cut-out location of the tensile test specimens is marked on the cross section of the barrel presented in Fig. 1 as 1. We performed four tensile tests for each material and used the average result of the measurements in the FEM model. The results are presented below in Table 2. The experimental determination of the tensile strength was carried out in a laboratory at a constant temperature of 23 °C.

Table 2 Results of tensile testing of materials A and B

Parameter	Material A [MPa]	Material B [MPa]
$R_{p0.2}$	1,217 ± 8	1,068 ± 16
R_m	1,303 ± 1	1,152 ± 13

2.3 Determining the fracture toughness of the materials

In accordance with the ASTM E399 standard [17] we performed experimental measurements of K_{IC}. For each material three side-notched specimens were cut from the disc of a barrel and tested using the machine INSTRON1225. The location of samples is as similar as possible to the location of the crack that was then simulated in the model. In Fig. 1, the samples are marked as 2. The K_{IC} factor is determined as an average of three successful measurements. The measured average values are 151.4 MPa·$m^{1/2}$ for material A and 151.1 MPa·$m^{1/2}$ for material B. All the results are shown in Table 3. We can conclude that no significant difference can be observed between the two materials.

Table 3 Experimental results of stress intensity factor. Units are in MPa·$m^{1/2}$

Parameter	Sample 1	Sample 2	Sample 3	Average Value
K_{IC}^{A}	150.51	151.85	151.76	151.37
K_{IC}^{B}	157.21	151.71	147.87	151.10

Based on the experimentally determined value of K_{IC}, we can determine the critical depth of the crack for individual materials.

3. Finite element modelling of a howitzer cannon barrel

The model of a cannon barrel without and with a semi-elliptical crack was created in Abaqus/CAE version 6.14, a FEM software, which enables two different approaches to model structures with cracks. In our model, due to the possibility of using symmetry, we used a classical approach where it is necessary to define the crack front, but in the literature, we can also find the XFEM approach for solving a similar problem, which is intended to study crack propagation [18, 19].

We have considered a longitudinally oriented crack, because such a configuration is more dangerous for further expansion than the radially oriented one. The shape of the crack is defined by the ratio *a/c*, where the parameter *a* represents the depth of the crack, and the parameter *c* its half-width. The geometry of the used barrel is presented in Table 4. The wall thickness *T* is the thickness at the place where we simulated the crack. The depth of the crack, expressed by the *a/t* ratio, was between 0.03 and 0.13.

Table 4 Parameters that determine the barrel geometry. Units are in mm

Parameter	R_i	R_o	T	L
Value	77.5	170.5	93	8140

3.1 Material properties

When defining the material properties, we used the elasto-plastic properties. Based on the experimentally obtained stress-strain curve *σ(ε),* we defined Young's modulus $E^A = 200.0 \cdot 10^3$ MPa and $E^B = 205.7 \cdot 10^3$ MPa and determined the yield strengths $R^A_y = 1097$ MPa and $R^B_y = 1031$ MPa. Ten points were taken from the area between R_y and the tensile strength of the materials R_m, and after the conversion into actual stress and strain, they were used in the model. For both material behaviours, we considered isotropic hardening and a value of Poisson's ratio of 0.3.

3.2 Pressure distribution and boundary conditions

The shape of the pressure value curve depending on the position in the cannon barrel is based on the description in [20], where the maximum pressure value is $p_{max} = 380$ MPa. Based on the literature, the maximum pressure values were extended to the range between 300 MPa and 420 MPa [4-5, 21-24]. To obtain the entire $p(x)$ curve, we normalized the p_{max} values of the curve from [20], which is shown in Fig. 2.

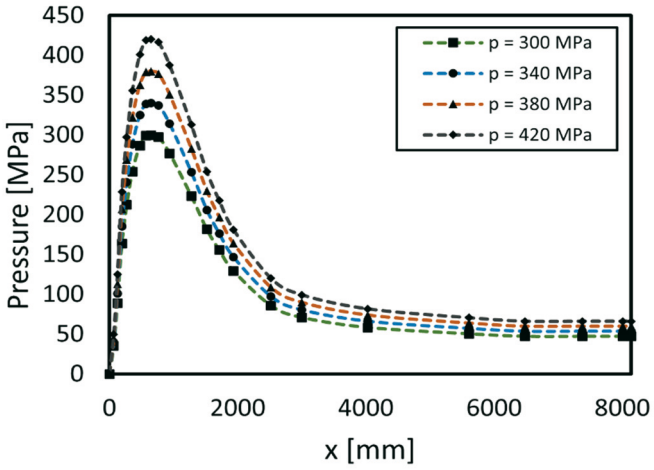

Fig. 2 Distribution of pressures $p(x)$ with different values of maximum pressure p_{max}

We divided the curves into three sections for better fitting of the polynomial functions to the individual section. The first section describes the barrel in the range of $x_1 = [0, 1700]$ mm,

the second section describes the range of x_2 = [1700, 5600] mm and the third section describe the range of x_3 = [5600, 8140] mm. The degrees of the used polynomials are quartic in the case of the first two sections and linear in the case of the third section, which is also the least important for this study.

Due to the symmetry of the problem, we only modelled one half of the model, thereby drastically saving the computation time of the simulation. We used three boundary conditions, symmetry in one direction (*XSYMM*), and two boundary conditions with which we fixed the model in the remaining two directions, *U2*=0 and *U3*=0. The boundary conditions for fixing the model were considered only at the extreme point of the geometry, while for the symmetry of the model we chose the entire cross-sectional area with the exception of the crack location. As for the type of crack, we used the contour integration, and the second contour was chosen as a crack front (Fig. 3). Crack propagation was defined with the normal to the crack plane.

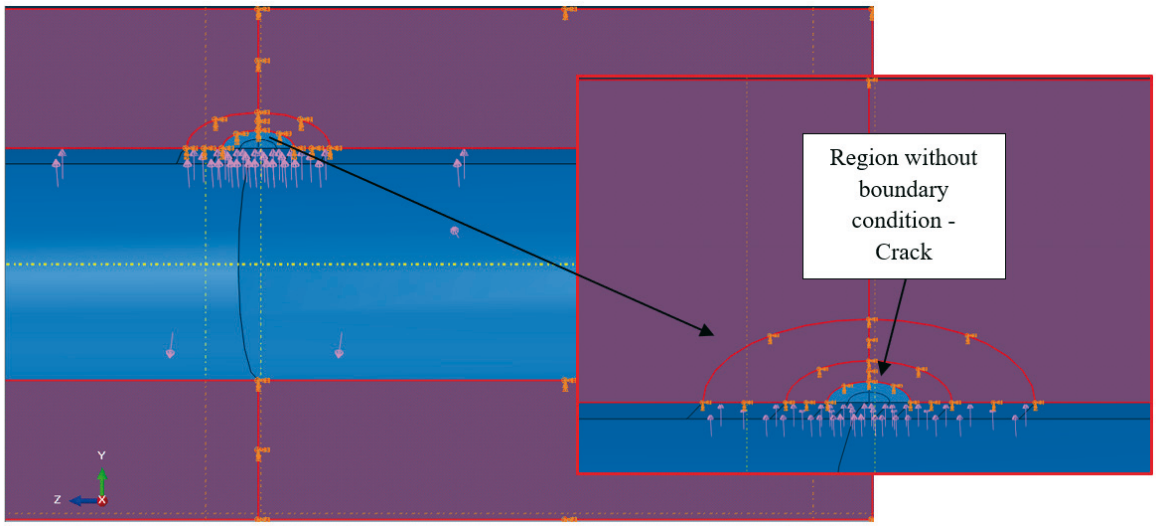

Fig. 3 Symmetric boundary conditions of the model except for the area of crack location. The figure shows a crack with a = 6 mm and ratio a/c = 0.5

3.3 Meshing and elements

C3D8 type elements were used for meshing without reduced integration [25]. A similar approach and meshing techniques were applied in the punch test [26, 27]. The size of the elements was 10 mm on the thicker part of the barrel to be gradually increased along the length of the barrel. In the middle part of the barrel, the size of the elements was between 30 mm and 50 mm, and in the last part, where the stress field analysis is the least important, the size of the elements was between 100 mm and 200 mm. At the crack location, we used element sizes from d_e = [0.15, 0.3, 0.45, 0.6] mm, and the ratio between the crack depth a and the element size d_e was always equal to 20, a/d_e = 20.

To get a better mesh quality, we divided the model with three additional contours, parallel to the contour that was chosen for the crack front. One contour was smaller than the contour of the crack front, and two were larger. The ratio between the size of the contour dimensions (c') was $c'_{i+1}/c'_i = 2$, where i = [1, 2, 3] is an index indicating the consecutive number of the contour by size.

The final meshing was performed gradually, for each segment of the model separately. The total number of elements for the crack with the ratio a/c = 1 was between $226 \cdot 10^3$ and $256 \cdot 10^3$. The result of a different crack geometry with a parameter ratio a/c = 0.5 was a significantly higher number of elements, which was between $367 \cdot 10^3$ and $572 \cdot 10^3$. The shape of the elements around the crack tip can be seen in Fig. 4. The meshing of details for both aspect ratios is shown in Fig. 6.

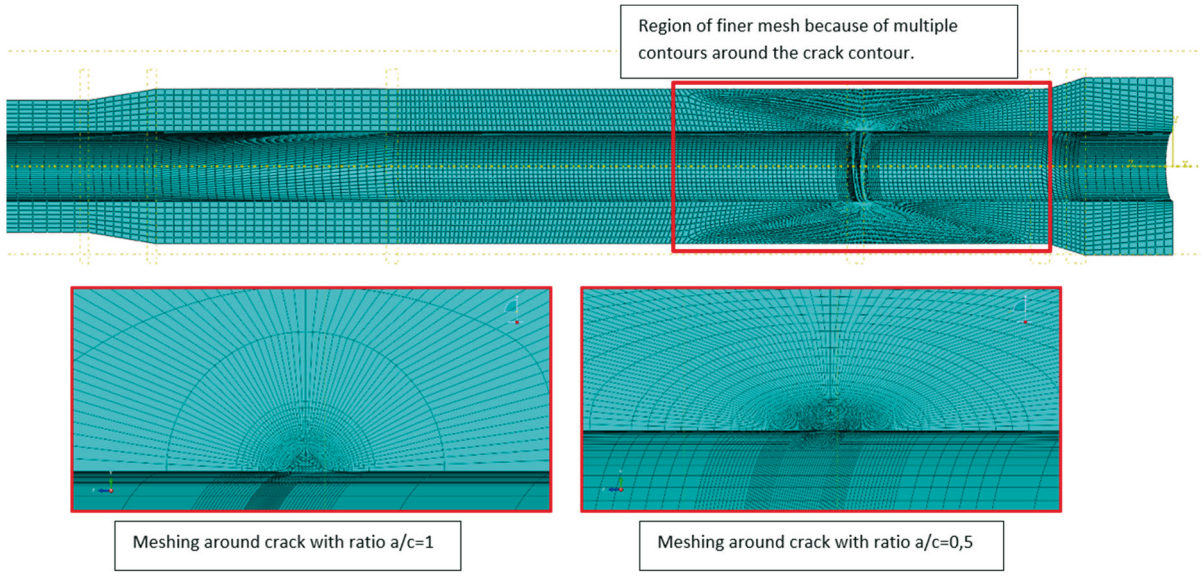

Fig. 4 Meshing of the thicker part of the barrel where the crack is located and meshing of details for ratios $a/c = 1$ and $a/c = 0.5$

4. Results

4.1 Validation of the FEM model

In the first step, we performed simulations of the pressure in the howitzer cannon barrel without considering the crack, to validate the model through the stress field. In Fig. 5 we can see the stress field expressed in the form of hoop stresses σ_h for the applied pressure function which peaks at 380 MPa.

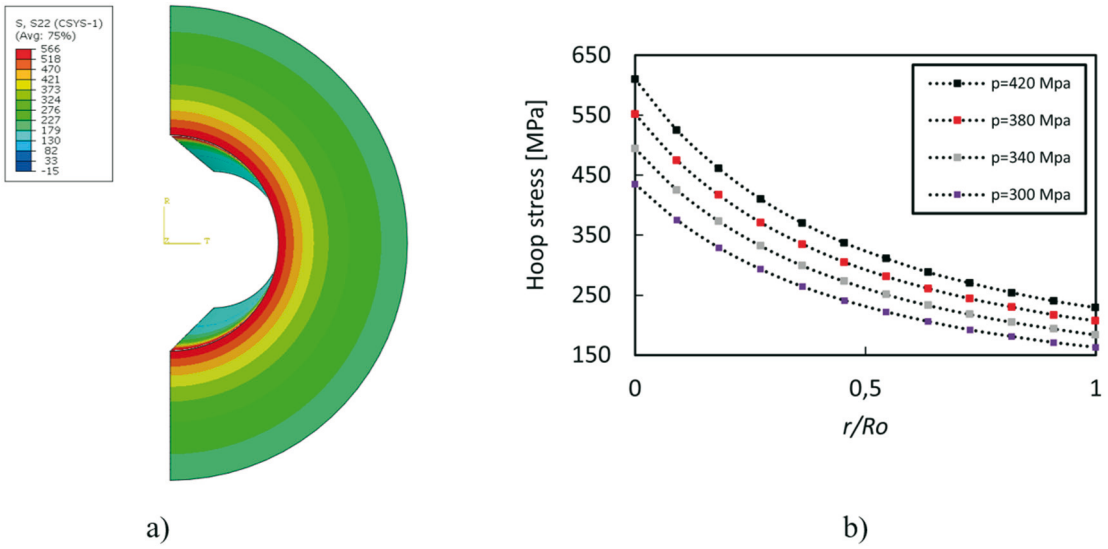

Fig. 5 a) Stress field in the barrel with maximum pressure value of $p_{max} = 380$ MPa; b) Distribution of hoop stresses along the thickness of the barrel at the location of the simulated crack

In this step, we conducted four simulations with maximum pressures ranging from 300 MPa to 420 MPa. The objective was to assess and evaluate σ_h, which are crucial for the crack propagation analysis. We compared the value of the simulated stress at the point of the maximum pressure to the analytically calculated values at the location of the inner wall, R_i.

The analytically calculated value of σ_h at the maximum pressure p_{max}=380 MPa is 577 MPa, while the simulation returns the value of 564 MPa, so the difference between the

analytical calculation and our model is approximately 2%. A slightly higher value of the stress of the simulation is expected since the elements at R_i are affected by the neighbouring elements. Fig. 5b shows the distribution of σ_h along the barrel cross section for all used pressure distributions, with the normalized value of the radius, r/R_o, on the abscissa.

4.2 Stress field in the proximity of the crack tip

After completing the validation of the model without cracks, we proceeded with simulating the model with cracks. We analysed four different crack depths, a = [3, 6, 9, 12] mm with two different ratios a/c = [0.5, 1]. For each ratio, at a specific crack depth, simulations were conducted at maximum pressures p_{max} = [300, 340, 380, 420] MPa. Consequently, the total number of simulations amounted to 64 due to the analysis of two different materials (graphs in Figs. 7 and 8).

Fig. 6 illustrates an example of the Von Misses stress field at a crack depth of a = 3 mm and p_{max} = 300 MPa. Figs. 6a) and 6b) depict the stress field at the cross section of the crack. In this part of the analysis, we can observe that the stress field surrounding the crack at the ratio of a/c = 0.5 reaches higher values compared to the stress field around the crack at the ratio of 1. The maximum value of Von Misses stresses at the crack with an a/c ratio of 1 is 1282 MPa, whereas this value is significantly higher at the crack with an a/c ratio of 0.5 and at 1651 MPa. The stress data clearly indicates that the crack shape with an a/c ratio of 0.5 is more critical in terms of further crack propagation, as also revealed in further analysis (Chapter 4.3).

Since our problem is symmetrical, we mirrored the model to analyse the stress field around the crack on the inner wall of the cannon barrel. Figs. 6c) and 6d) display a comparison of the stress field around the open crack. For the presentation of these results, we used a deformation factor of 50, which more clearly illustrates the opening of the crack.

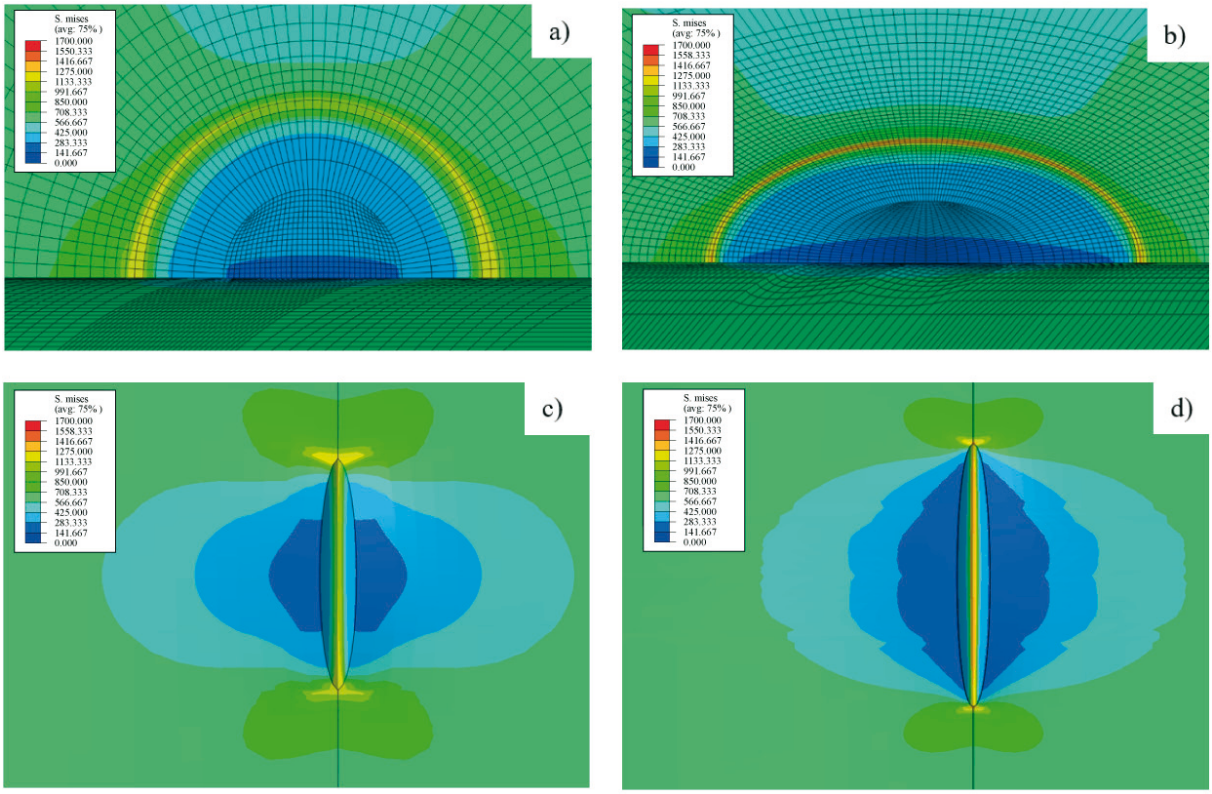

Fig. 6 Von Misses stresses in the unit MPa in the surroundings of two different semi-elliptical cracks of depth a=3 mm and inner barrel pressure of 300 MPa; a) Cross section of crack with ratio a/c=1; b) Cross section of crack with ratio a/c=0.5; c) Stress state on global model for crack with ratio a/c=1; d) Stress state on global model for crack with ratio a/c=0.5

4.3 Stress intensity factor along the crack tip

With the help of the FEM model we can determine K_I for the elements contained in the contour of the crack tip. To determine the value of K_I, we chose the energy approach, where we first determine the so-called *J*-integral. The determination of the value is based on the integration of the energy domain in the vicinity of the crack tip. The equation that describes the calculation of the *J*-integral was derived by Shih et al. [28] as follows:

$$J = \int_A \left(\sigma_{ij} \frac{\partial u_j}{\partial u_x} - w \partial u_i \right) \frac{\partial \mathrm{q}}{\partial \mathrm{x_i}} \mathrm{d}A \tag{1}$$

where A is the surface between the contours Γ_0 and Γ_1, the parameter q is a smoothed function and can have the value $q = 1$ on Γ_0 and $q = 0$ on Γ_1.

In practice, the tip of the crack is chosen for Γ_0 [18]. Further discretization of Eq. 1 can be written as:

$$J = \sum_A \sum_{p=1}^{n'} \left(\left[\left(\sigma_{\mathrm{ij}} \frac{\partial u_{\mathrm{j}}}{\partial u_{\mathrm{x}}} - w \partial u_{\mathrm{i}} \right) \frac{\partial q}{\partial x_{\mathrm{i}}} \right] \det \left(\frac{\partial x_j}{\partial \xi_k} \right) \right) w_{\mathrm{p}} \tag{2}$$

where n' is the number of Gaussian points, w_p is the integration weight and ξ_k are the local coordinates of the elements. K_I was then determined using the equation derived by Rice [29]:

$$K_{\mathrm{I}} = \sqrt{JE'} \tag{3}$$

where J is the value of the *J*-integral, $E'=E/(1-\nu^2)$ is Young's modulus for plane strain state and ν is Poisson's number.

On the graphs presented in Figs. (8a-h) and (9a-h) we can see the distribution of K_I at the crack tip for the ratios $a/c = 1$ and $a/c = 0.5$ for the considered materials, and the applied pressures p_{max} = [300, 340, 380, 420] MPa. On the abscissa we use the value x/c, which is the normalized coordinate of the crack with the value 0 at the location of the maximum crack depth. On the graphs, the experimentally determined critical value of K_{IC} is marked with a dashed red line. The shapes of the curves match the shapes of the curves given in other studies [30, 31] and of the theoretical prediction, which is described for the deepest point of the crack by the following equation:

$$K_{\mathrm{a}} = f(a) = F \cdot \sigma_{\mathrm{H}} \cdot \sqrt{\pi a} \cdot 0.97 \cdot \left(\frac{R_{\mathrm{o}}^2 + R_{\mathrm{i}}^2}{R_o^2 - R_{\mathrm{i}}^2} + 1 - 0.5 \sqrt{\frac{a}{t}} \right) \cdot \frac{t}{R_{\mathrm{i}}} \tag{4}$$

where $t = R_o - R_i$ is the wall thickness, σ_H is the hoop stress and F is the factor expressed as:

$$F = \frac{M_1 + M_2 \cdot \left(\frac{a}{T} \right)^2 + M_3 \cdot \left(\frac{a}{T} \right)^4}{\sqrt{Q}} \tag{5}$$

where $M_1 = 1.13 - 0.09(a/c)$, $M_2 = -0.54 + (0.89/(0.2+a/c))$, $M_3 = 0.5\text{-}1/(0.65+a/c)+14(1-a/c)^{24}$ and $Q=1+1.464(a/c)^{1.65}$.

It can be seen that the difference between the two materials used in the simulation is almost negligible. In the case of the ratio $a/c = 1$, the maximum difference in the stress intensity factor at the deepest point of the crack, K_a, is $K^A_a - K^B_a = -2.9$ MPa·m$^{1/2}$ at pressure p_{max} = 420 MPa, and the minimum difference is −1.0 MPa·m$^{1/2}$. In the case of the ratio

a/c = 0.5, the minimum and maximum differences occur at the same pressures; in this case they are −3.2 MPa·m$^{1/2}$ and −1.3 MPa·m$^{1/2}$, respectively. Despite the small difference, we can see that K_I reaches higher values in material B than in material A, which means that material A is more resistant to the propagation of cracks under high loads on the inner wall of the barrel during the operation of a howitzer.

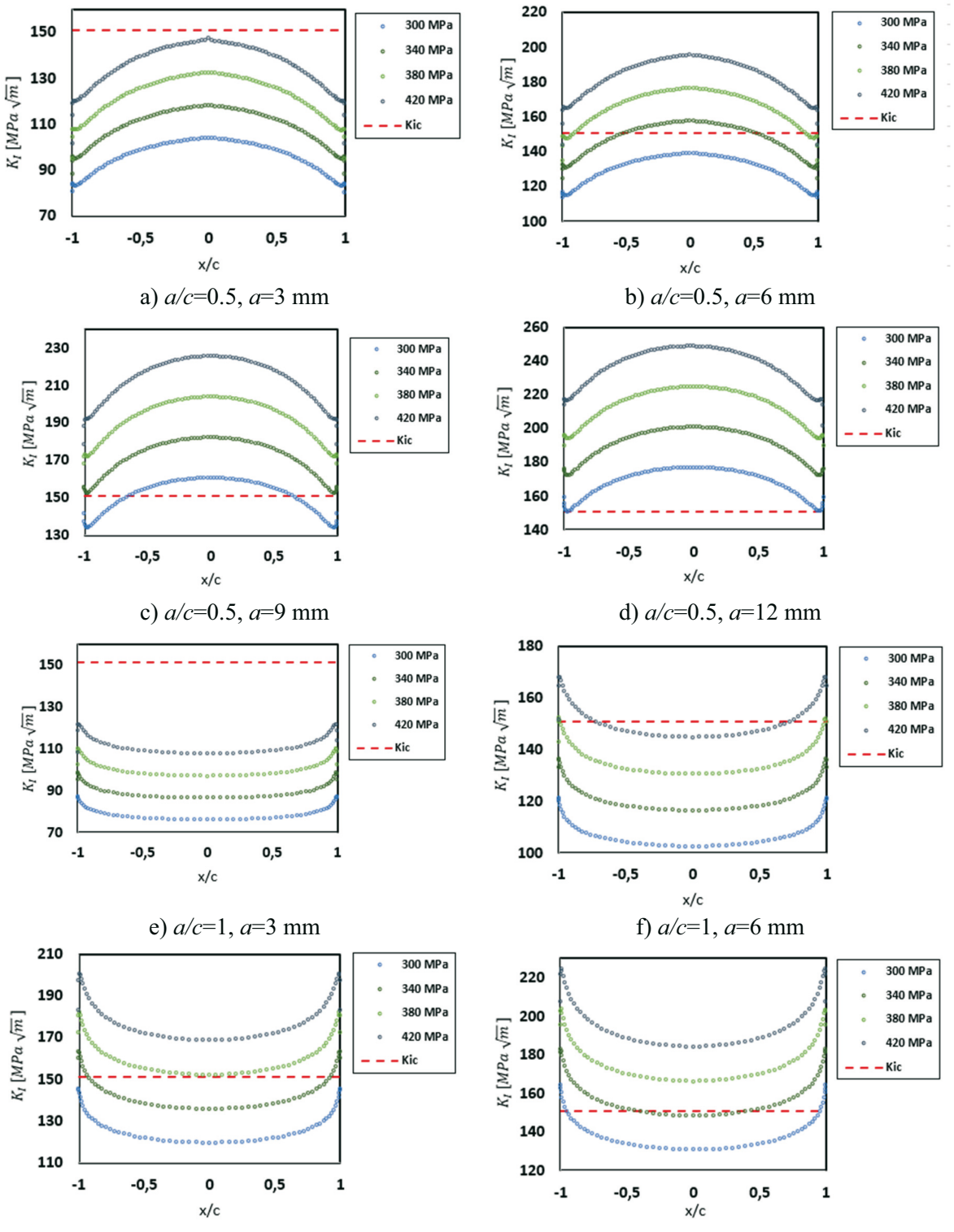

a) a/c=0.5, a=3 mm

b) a/c=0.5, a=6 mm

c) a/c=0.5, a=9 mm

d) a/c=0.5, a=12 mm

e) a/c=1, a=3 mm

f) a/c=1, a=6 mm

g) a/c=1, a=9 mm

h) a/c=1, a=12 mm

Fig. 7 Values of stress intensity factor along crack tip for material A at ratio a/c = 0.5 and a/c=1

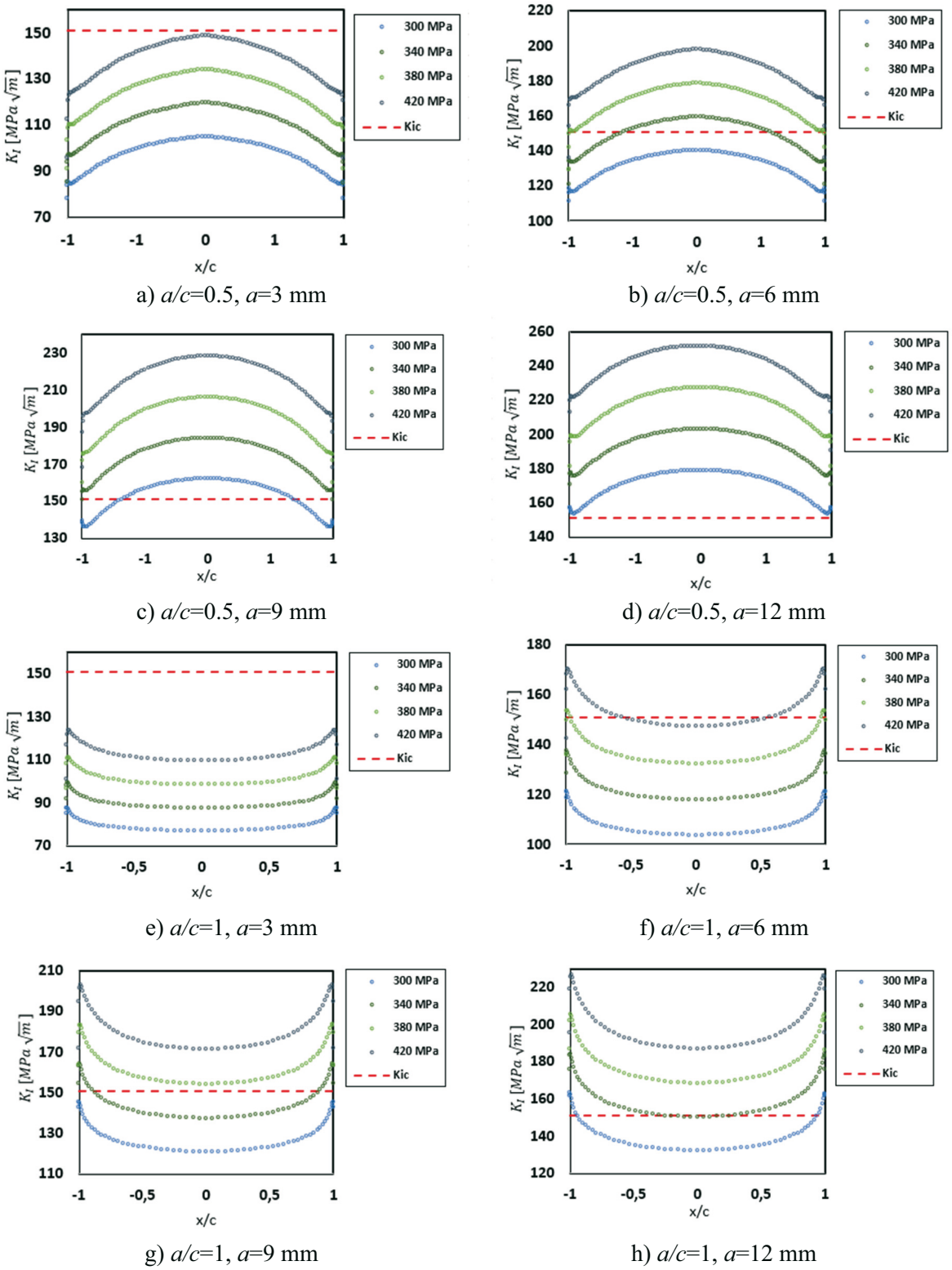

a) a/c=0.5, a=3 mm

b) a/c=0.5, a=6 mm

c) a/c=0.5, a=9 mm

d) a/c=0.5, a=12 mm

e) a/c=1, a=3 mm

f) a/c=1, a=6 mm

g) a/c=1, a=9 mm

h) a/c=1, a=12 mm

Fig. 8 Values of stress intensity factor along crack tip for material B at ratio a/c = 0.5 and a/c=1

4.4 Determination of the critical pressure in a cannon barrel with a crack

In general, when constructing a FAD, the main function is $f(L_r)$, which describes the acceptability of a crack on the structure taking the change in plasticity at the tip of the crack into account. A crack on a structure is acceptable until the stress intensity factor at the tip of the crack reaches a critical value:

$$K_{\mathrm{r}} \le f\left(L_{\mathrm{r}}\right) \tag{6}$$

where L_{r} is the normalized load defined as:

$$L_{\mathrm{r}} = \frac{\sigma_{\mathrm{app}}}{\sigma_{\mathrm{y}}} \tag{7}$$

where σ_{app} is the stress due to the external load. The normalized load defines the degree of plastification which the design material is exposed to:

$$L_{\mathrm{r}} = \frac{\sigma_{\mathrm{app}}}{\sigma_{\mathrm{y}}} = \frac{p_{\mathrm{app}}}{p_{\mathrm{y}}}\ , \tag{8}$$

where p_{app} is the external load expressed by pressure and p_{y} is the limit load expressed by the pressure at the yield point, which considers the size of the crack. When the R6 approach is applied to barrel with a semi-elliptical crack in the longitudinal direction, p_{y} can be written as:

$$\frac{p_{\mathrm{y}}}{\sigma_{\mathrm{y}}} = \frac{\alpha\eta}{\left(1-\frac{1}{2}\eta\right)M_{\mathrm{g}}} + \frac{1-\frac{1}{2}\eta}{1-\frac{1}{2}\eta+\alpha\eta}\cdot\ln\left(\frac{1+\frac{1}{2}\eta}{1-\frac{1}{2}\eta+\alpha\eta}\right) \tag{9}$$

where:

$$M_{\mathrm{g}} = \sqrt{1+1.05\cdot\frac{\alpha\eta}{\Phi^2\left(1-\frac{1}{2}\eta\right)}} \tag{10}$$

and $\alpha=a/t$, $\eta=2t/(R_{\mathrm{i}}+R_{\mathrm{o}})$, $\varphi=a/c$ [30].

The plasticity correction function *f(Lr)* for the range $0 \le L_{\mathrm{r}} < 1$ is described by the following equation:

$$f\left(L_{\mathrm{r}}\right) = \left(1+\frac{1}{2}L_{\mathrm{r}}^2\right)^{-\frac{1}{2}}\left(0.3+0.7e^{-\mu L_r^6}\right) \tag{11}$$

with the value of the factor $\mu = \min(10^{-3}\ E/R_{\mathrm{p0.2}},\ 0.6)$. In the range between 1 and $L_{\mathrm{r}}^{\max}$ the plasticity correction function is written as:

$$f\left(L_{\mathrm{r}}\right) = f\left(L_{\mathrm{r}}=1\right)L_{\mathrm{r}}^{\frac{N-1}{2N}} \tag{12}$$

with the quantities

$$N = 0.3\left(1-\frac{R_{\mathrm{p0.2}}}{R_{\mathrm{m}}}\right) \tag{13}$$

and

$$L_{\mathrm{r}}^{max} = 0.5\cdot\frac{R_{\mathrm{p0.2}}+R_{\mathrm{m}}}{R_{\mathrm{p0.2}}}. \tag{14}$$

The normalized value of K_r is a parameter that gives the relationship between the stress intensity factor and the fracture toughness of the material as follows:

$$K_r = \frac{K_I}{K_{mat}}, \tag{15}$$

where K_I is the stress intensity factor of the loaded component with a crack and K_{mat} is the fracture toughness of the material [32, 33]. In the case of unstable fracture K_{mat} is equal to K_{IC}, which is determined experimentally according to the procedure of the ASTM E399 standard [17].

In this paper, we focus on the deepest point of the crack, which is at depth a, measured from the inner wall. At this point, the stress intensity factor is denoted as K_a, which means that the normalized value of the stress intensity factor K_r can be written as:

$$K_r = \frac{K_a}{K_{IC}} \tag{16}$$

The K_a factor was obtained by the FEM analysis of the howitzer barrel and can be seen in the graphs presented in Figs. (7a-h) and (8a-h). Based on Eq. 8 to Eq. 16, we constructed FADs for materials A and B, which can be seen in Fig. 9. For better clarity, we constructed an FAD for each of the materials for the ratios a/c = 0.5 and a/c = 1 separately.

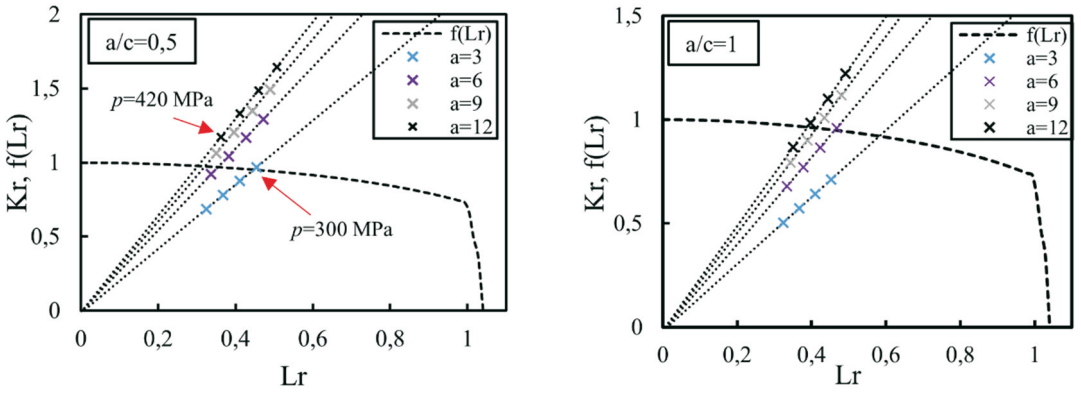

a) a/c=0.5, Material A

b) a/c=1, Material A

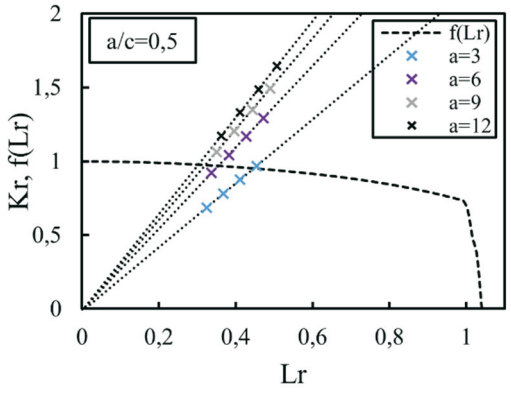

c) a/c=0.5, Material B

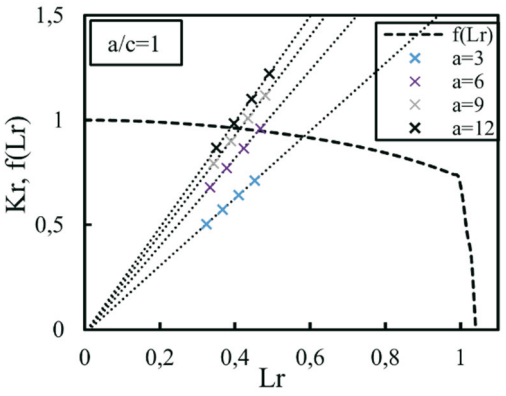

d) a/c=1, Material B

Fig. 9 FADs for a/c = 1 and a/c = 0.5

For each pressure p_{max} applied in the simulation four pairs (L_r,K_r) were obtained for a given crack depth a. The point closest to the coordinate origin belongs to the simulation with a pressure of p_{max} = 300 MPa, and the farthest point belongs to the simulation with a pressure of p_{max} = 420 MPa. The first thing that can be pointed out is that when considering the deepest point on the crack, the shape given by the ratio a/c = 0.5 is more dangerous than the shape given

by the ratio $a/c = 1$. This can be seen when comparing graphs (a) and (b) in Fig. 9. The crack of depth $a = 3$ mm already lies above the $f(L_r)$ curve for the applied pressure of 420 MPa at the ratio $a/c = 0.5$. This means that such condition would cause the crack to propagate. If we now compare this to the same conditions at the ratio $a/c = 1$, we can observe that for the crack to propagate the depth must be greater than 6 mm.

To determine the critical pressures more accurately for the considered crack lengths, we must fit linear functions to the pairs (L_r, K_r) and find the intersections of the functions with the curves $f(L_r)$. The intersection returns the value of L_r, which we can use to calculate the critical pressures shown in Table 5 using Eq. 8.

In Table 5, by calculating the critical pressure difference $\Delta p_{crit} = p^A_{crit} - p^B_{crit}$, we can once again see that material A is more resistant to further crack propagation for the two considered crack shapes. The maximum difference of 19 MPa occurs at the crack depth $a = 3$ mm and the ratio $a/c = 1$. The difference in the critical pressure in both forms decreases as the crack depth increases.

Table 5 Value of critical pressures for the considered crack depths. Pressure is expressed in MPa

a [mm]	3		6		9		12	
a/c	0.5	1	0.5	1	0.5	1	0.5	1
p^A_{crit}	414	539	317	417	276	364	363	334
p^B_{crit}	403	520	311	405	271	354	354	327
Δp_{crit}	11	19	6	12	6	9	4	7

4.5 Determination of the critical crack length

Usually, the data which we know or can simulate is the pressure distribution in the cannon barrel is caused by explosion. For this reason, it is important for the cannon barrel manufacturer to know what the critical depth or length of the crack are at a certain pressure. With the data obtained from the graphs (a-d) given in Fig. 9 we can construct a graph that gives the value of the critical depth of the crack which is dependent on the applied pressure. The depth of the crack a is used as the y-coordinate in the graph and the applied pressure represents the x-coordinate. Because of the use of two different materials and two different crack shapes, we get four sets of data to which we can apply a power function of the following form:

$$a_{crit} = C_1 \cdot p^{C_2} \tag{17}$$

The values of the coefficients C_1 and C_2 for both materials and crack shapes are shown in Table 6.

Table 6 Values of parameters C_1 and C_2 for constructing the power function

a/c	Material	$C_1 \cdot 10^8$	C_2
1	A	1.06	-2.77
	B	1.62	-2.85
0.5	A	0.28	-2.67
	B	0.37	-2.72

On the graph presented in Fig. 10 the pressure value of 380 MPa is marked with a red vertical line because this is the value that appears most often in the literature.

For material A, the value of the critical crack length a^A_{crit} at the ratio a/c is equal to 3.71 mm, which is comparable to the results presented in the papers where a cannon barrel was subjected to a pressure of 380 MPa [4-5, 8]. The critical lengths of the cracks in the mentioned papers are a_{crit} = [3.84, 3.74, 3.70] mm. For material B we can observe a slightly lower value of the critical crack length, $a^B_{crit} = 3.47$ mm, which is another indication that material A is more appropriate for cannon barrel production.

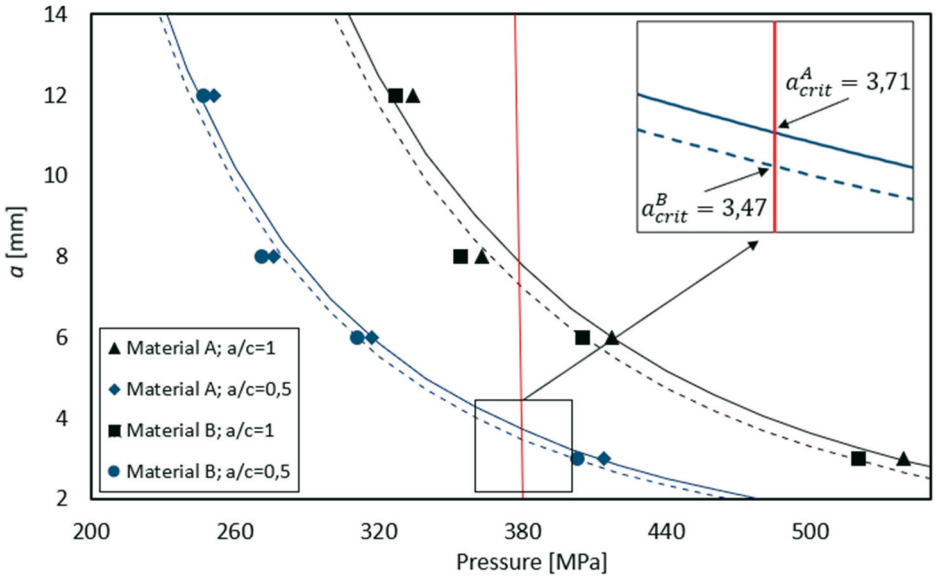

Fig. 10 Critical crack length as a function of cannon barrel pressure

5. Conclusion

In the conducted comprehensive analysis our focus centred on the comparative evaluation of two distinct heat treatments applied to the 35NiCrMoV12-5 material, emphasizing their impact on the fracture mechanical properties. Specifically, our investigation targeted K_I and its correlation with the critical crack depth.

The utilization of actual material data for materials A and B formed the basis of our FEM analysis applied to the cannon barrel. Our examination involved studying K_I at the crack tip within a symmetrical 3D model of the barrel. This analysis covered a study of different crack depths and shapes, evaluating the distribution of K_I across these variations.

The combination of the experimentally determined K_{IC} values and the results derived from the FEM model proved instrumental in the development of a comprehensive diagram, which is crucial for assessing the crack acceptability according to the R6 method. This method enabled the determination of critical pressures corresponding to the considered crack depths at the most critical location within the barrel.

Furthermore, we established power functions that described the critical crack length for specific pressure values. This process provided invaluable insights into predicting and evaluating critical crack lengths under different operational pressures, which is crucial for ensuring the structural integrity and safety of cannon barrels.

The culmination of these findings contributes to the field of fracture mechanics in the cannon barrel analysis. The systematic approach employed in this study underscores its importance in enhancing our understanding of the cannon barrel behaviour under stress, with implications extending to improved material selection and safety assessments in military applications.

Acknowledgements

The authors acknowledge the Slovenian Research Agency ARRS for partly funding this investigation in the frame of the research program P2-0137 “Numerical and Experimental Analysis of Nonlinear Mechanical Systems”.

REFERENCES

[1] H. Moustabchir, M. Alaoui, A. Babaoui, K. Dearn, C. Pruncu, and Z. Azari, "*The influence of variations of geometrical parameters on the notching stress intensity factors of cylindrical shells*" *Journal of Theoretical and Applied Mechanics*, vol. 55, pp. 559–569, 2017, https://doi.org/10.15632/jtam-pl.55.2.559

[2] M. Berer, I. Mitev, and G. Pinter, "Finite element study of mode I crack opening effects in compression-loaded cracked cylinders," Engineering Fracture Mechanics, vol. 175, pp. 1–14, 2017, https://doi.org/10.1016/j.engfracmech.2017.03.008

[3] A. Zareei and S. Nabavi, "Calculation of stress intensity factors for circumferential semielliptical cracks with high aspect ratio in pipes," International Journal of Pressure Vessels and Piping, vol. 146, pp. 32–38, 2016, https://doi.org/10.1016/j.ijpvp.2016.05.008

[4] R. Eliasi, L. Banks Sills, "Fatigue Life Analysis of a Cannon Barrel," Engineering Failure Analysis, 1999, https://doi.org/10.1016/S1350-6307(98)00054-5

[5] R. Mahdavinejad, "Prediction of Cannon Barrel Life," Journal of Achievements in Materials and Manufacturing Engineering, vol. 30, 2008.

[6] G. Fašun, N. Gubeljak, M.D. Chapetti, "Fatigue integrity analysis of a howitzer cannon by using a fracture mechanics approach", Engineering fracture mechanics, vol 292, 2023, https://doi.org/10.1016/j.engfracmech.2023.109672

[7] G. Fašun, N. Gubeljak, M.D. Chapetti, "*Fatigue life of a Howitzer cannon*", Procedia Structural Integrity, vol 48, 2023, https://doi.org/10.1016/j.prostr.2023.07.105

[8] C. Ian, L. Stan, "The dependency of Stress Intensity Factor to the Crack Length and Temperature of a Cannon Barrel Using the J-Integral", Conference paper, 2019.

[9] A. Bannister and S. Trail, "Structural integrity assessment procedures for European industry," British steel plc, 1996.

[10] K.-H. Schwalbe, U. Zerbst, Y. Kim, W. Brocks, A. Cornec, J. Heerens, and H. Amstutz, "EFAM ETM 97 - The ETM method for assessing the significance of crack-like defects in engineering structures, comprising the versions ETM 97/1 and ETM 97/2," GKS, Germany, 1998.

[11] BS 7910, "Guide to Methods for Assessing he Acceptability of Flaws in Metallic Structures," British Standards Institutions, London, UK, 2013.

[12] B.P.F. Procedure, "R6 Revision4: Assessment of the integrity of structures containing defects," British Energy Gloucester, UK, 2024.

[13] P.J. Buden, J. K. Sharples, "The R6 Defect Assessment Procedure: Status and Key Recent Developments," SMiRT-23, Manchester, UK, 2015.

[14] Ahmad, Shahnawaz & Kumar, Vikas, "Structural Integrity Analysis of a Battle Tank Gun Barrel during Service", Defence Science Journal, 2015, https://doi.org/10.14429/dsj.65.7800

[15] Metal Ravne, SIQUAL 6959 Steel (Mat.No. 1.6959, DIN 35NiCrMoV12-5)." https://steelselector.sij.si/steels/KATO1.html (Accessed Dec. 17, 2022).

[16] ASTM International "ISO 6892-1(2019): Metallic materials -Tensile testing - Part 1: Method of test at room temperature," 2019.

[17] ASTM International, "ASTM E399-20a: Standard test method for linear-elastic plane-strain fracture toughness of metallic materials," 2022.

[18] S. El Fakkoussi, H. Moustabchir, A. Elkhalfi, and C. Pruncu, "Computation of The Stress intensity Factor Ki For External Longitudinal Semi-Elliptic Cracks In The Pipelines By FEM And XFEM Methods," International Journal on Interactive Design and Manufacturing (IJIDeM), vol. 13, 2019, https://doi.org/10.1007/s12008-018-0517-1

[19] S. Montassir, K. Yakoubi, H. Moustabchir, A. Elkhalfi, D. Rajak, and C. Pruncu, "*Analysisof Crack Behaviour in Pipeline System Using Fad Diagram Based on Numerical Simulation Under XFEM*," Applied Sciences, vol. 10, p. 6129, 2020, https://doi.org/10.3390/app10176129

[20] O. Gungor, "An Approach for Optimization of The Wall Thickness (Weight) Of A Thick-Walled Cylinder Under Axially Non-Uniform Internal Service Pressure Distribution," Defence Technology, vol. 13, pp. 150–157, 2017, https://doi.org/10.1016/J.DT.2017.04.003

[21] J.J. Ritter, B.E. Homan, W. Thalman, Dynamic Pressure Testing of a 155-mm Howitzer Ballistic Window Using a Closed Bomb Vessel, Research report, Adelphi, USA, Aug. 2010.

[22] D. Carlucci, J. Vega, Empirical relationship for muzzle exit pressure in a 155 mm gun tube, *WIT Transactions on Modelling and Simulation*, vol. 45, pp. 225–229, 2007, https://doi.org/10.2495/CBAL070211

[23] W. You, T. Ma, Y. Ding, M. Cui, Simulated artillery chamber pressure generator for special dynamic evaluation, *Automatics*, vol. 57, no. 2, pp. 525–531, Jan. 2016, https://doi.org/10.7305/automatika.2016.10.1105

[24] Ravne Systems d.o.o., Technical requirements for production, control, testing and acceptance of gun barrel assembly, Technical report, Ravne na Koroškem, Slovenia, Sept. 1999.

[25] "ABAQUS/Standard User's Manual, Version 6.9," USA: Dassault Systemes Simulia Corp, 2009.7

[26] K. Ganesan, S. Sambasivam, R. Ramadass, Determination of Limiting Dome Height (LDH) values for Inconel 718 alloy sheet using FEA and Hemispherical Punch Method. Strojniški vestnik - Journal of Mechanical Engineering, [S.l.], v. 68, n.6, p. 439-448, may 2022. ISSN 0039-2480. https://doi.org/10.5545/sv-jme.2022.98

[27] Zhou Q. H., Qiu Y. H., Liu H. S., He, Y. (2023). A Performance Study on Structural Parameters of Centre-Axle-Trailer Combinations. *Int. Journal of Simulation Modelling*, Vol. 22, No. 1, p. 168-179 https://doi.org/10.2507/IJSIMM22-1-CO5

[28] C. Shih, B. Moran, and T. Nakamura, "*Energy Release Rate Along a Three-Dimensional Crack Front in A Thermally Stressed Body*," International Journal of Fracture, vol. 30, pp. 79–102, 1986, https://doi.org/10.1007/BF00034019

[29] J. R. Rice, "A Path Independent Integral and the Approximate Analysis of Strain Concentration by Notches and Cracks," Journal of Applied Mechanics, vol. 35, p. 379, 1968, https://doi.org/10.1115/1.3601206

[30] E. Atroshchenko, S. Potapenko, G. Glinka, "*Stress Intensity Factor for A Semi-Elliptical Crack Subjected to An Arbitrary Mode I Loading*," Mathematics and Mechanics of Solids, vol. 3, 2014, https://doi.org/10.1177/1081286512463573

[31] S. Wang, B. Wang, Y.-J. Janin, R. Bourga, and H. Xue, "*Effects of The Surface Crack Shape on J Values Along the Front of an Elliptical Crack*," Fatigue & Fracture of Engineering Materials & Structures, vol. 44, no. 11, pp. 2944–2961, 2021, https://doi.org/10.1111/ffe.13522

[32] M. Kocak, S. Webster, J. Janosch, R. Ainsworth, R. Koers, "*FITNET Fitness-For-Service Procedure–Final Draft MK7*," FITNET FFS–MK, vol. 7, 2006.

[33] C. M. Sonsino and R. Rennert "Comparison of two equivalent stress methods based on cumulative damage adjustment and on a consistent fatigue strength reduction for transforming of variable into constant amplitude loading" *Materials Testing*, vol. 65, no. 5, 2023, https://doi.org/10.1515/mt-2022-0373

Submitted: 16.12.2023

Accepted: 05.3.2024

Gašper Fašun
SIJ Ravne Systems d.o.o.,
Ravne na Koroškem, Slovenia
Jožef Predan
Nenad Gubeljak*
Faculty of Mechanical Engineering,
University of Maribor, Maribor, Slovenia
*Corresponding author:
nenad.gubeljak@um.si